



RADIATION SHIELDING FEATURES OF GLASS FIBER REINFORCED CAST POLYAMIDE USING PHY-X/PSD AND SRIM SOFTWARE

Jeevan Poudel, Basanta Subedi, Tika Ram Lamichhane*

Central Department of Physics, Tribhuvan University, Kirtipur, Kathmandu, Nepal, Nepal

*Correspondence: tika.lamichhane@cdp.tu.edu.np

(Received: June 06, 2023; Final Revision: September 15, 2023; Accepted: December 23, 2023)

ABSTRACT

The utilization of various materials for their nuclear radiation shielding properties has been the subject of a growing number of research and development projects. In this study, the radiation shielding characteristics of E-glass fiber reinforced cast polyamide were evaluated. E-glass is a form of glass fiber frequently utilized as a reinforcement in various composite materials to provide more durability, stiffness, and strength. Samples S1-S7 were defined according to various compositions of E-glass fiber contents (SiO_2 , Al_2O_3 , B_2O_3 , MgO , CaO , Na_2O and K_2O) and cast polyamide ($\text{C}_{12}\text{H}_{22}\text{N}_2\text{O}_2$). Within the energy range 0.015-15 MeV, the shielding parameters: Linear attenuation coefficient (LAC), mass attenuation coefficient (MAC), half and tenth value layers (HVL, TVL), mean free path (mfp), effective atomic number (Z_{eff}), atomic and electronic cross sections (ACS, ECS), fast neutron removal cross-section (FNRCs) and exposure buildup factor (EBF) were analyzed. E-glass fiber reinforced cast polyamide S7 (70% glass fiber content) exhibited higher values of LAC, MAC and Z_{eff} and lower values of HVL, TVL, and mfp proving it to be a better radiation shielding material among the samples. An abrupt reduction in values of Z_{eff} was discerned within the photoelectric absorption-dominant region, contrasted with a stable trend within the Compton scattering-dominant region, and a marginal elevation was noted in the pair production region. The maximum and minimum values of FNRCs were observed for samples S1 (10% glass fiber content) and S5 (50% glass fiber content) respectively. Hence, S1 would be the most effective material in fast neutron shielding. At 35 mfp penetration depth, the minimum EBF values belonged to S7 in lower and intermediate regions (0.015-3 MeV) whereas S1 showed the minimum values at higher energy regions (4-15 MeV). Furthermore, the mass stopping power (MSP) and projected range (PR) of the samples for alpha and proton particles were determined using SRIM-2008 codes. S7 exhibited better shielding features for alpha and proton particles with lower values of mass stopping power and projected range. The reinforcement of glass fiber in the cast polyamide has been noticed to have a significant impact on the shielding performance of polymer composites.

Keywords: Glass fiber reinforced cast polyamide, Phy-X/PSD, radiation shielding parameters, SRIM, ion interactions

INTRODUCTION

With a wide range of applications, including power plants, space exploration, agriculture, and medicine, the usage of radioactive sources has grown tremendously. Longer exposure to the penetrating photon beams released by the radioactive source has the potential to harm both the environment and living beings. Thus, using shielding materials has become essential for minimizing these detrimental health impacts. Physicists find this area of study to be attractive due to the radiation shielding properties of materials and comparative studies with existing shielding materials.

The well-known element utilized for radiation shielding applications is lead (Pb). However, new types of protective materials that do not include lead must be developed due to some of its restricted characteristic qualities such as weak mechanical strength, and toxicity. Designing new shielding materials with properties like good mechanical strength, high transparency, and low cost is crucial for this purpose (Sakar *et al.*, 2020; More *et al.*, 2021). Due to the lightweight, durability, flexibility, and superior physical, mechanical, optical, and radiation resistance capabilities, polymer and its composites offer promising acceptable alternatives to lead and concrete in

the field of radiation shielding (Ambika *et al.*, 2017; Alavian *et al.*, 2020). Among the silicon polymers such as polymer A-poly dimethyl siloxane ($\text{C}_2\text{H}_6\text{OSi}$), polymer B-polymethyl hydro-siloxane (CH_4SiO), polymer C-per hydro-polysiloxane (H_3SiN), polymer D-poly dimethyl siloxane ($\text{C}_2\text{H}_6\text{Si}$), polymer E-methylsiloxane quinoxaline ($\text{C}_{12}\text{H}_{32}\text{O}_8\text{Si}_8$), and polymer F-silalkylene polymer (SiC_3H_8), it was found that polymethyl hydro-siloxane (CH_4SiO) possessed the lowest values of half value layer (HVL), tenth value layer (TVL) and mean free path (mfp) and the highest attenuation coefficient (Nagaraja *et al.*, 2020). The radiation effect of ^{60}Co gamma rays on a polycarbonate detector was studied using a spectrophotometric method and the results showed that the polycarbonate had good performance to be employed as a gamma radiation dosimeter (Galante and Campos, 2010). Due to its qualities including its transparency, ease of manufacturing, non-toxicity, and high density, glasses also have recently been investigated as an alternative radiation shielding material (Hussein *et al.*, 2022). Several research have been carried out to investigate the radiation shielding properties of various glass systems: for glasses with high Bi_2O_3 concentration (El-Denglawey *et al.*, 2021); for tellurite glasses (El-

Mallawany, 2018); for barium borate glasses (Al-Buriah *et al.*, 2020).

This research is focused on the radiation shielding features of glass fiber reinforced cast polyamide. By several orders of magnitude, E-glass fibers are the most often utilized fibrous reinforcement material. Affordability and rapid development raise the importance of these materials in comparison to other fibers. E-glass fiber reinforced cast polyamide was observed to have mechanical properties such as tensile strength and modulus of elasticity increased when the fiber volume content is increased up to 35%. However, these properties decreased at the fiber content higher than that of 35% (Cuvalci *et al.*, 2014). These eco-friendly cast polyamide-based composites could be an alternative to existing radiation shielding materials at lower photon energies.

The software employed in the calculation of shielding parameters is Phy-X/PSD (Photon Shielding and Dosimetry) running on a remote server that has Intel® Core(TM) i7-2600 CPU @ 3.40 GHz CPU with 1 GB installed memory and the operating system is Ubuntu 14.04.3 LTS (Sakar *et al.*, 2020). For the calculations of mass stopping power (MSP) and projected range (PR), SRIM-2008 codes have been used. SRIM is abbreviated for Stopping and Range of Ions in Matter. The SRIM software suite uses a quantum mechanical analysis of ion-atom collisions to determine the stopping power and range of ions (up to 2 GeV/amu). The use of statistical techniques that allow the ion to bounce between computed collisions and then average the collision outcomes over the subsequent pause makes this calculation exceedingly efficient (Ziegler *et al.*, 2010).

A monoenergetic beam's incoming photon fraction per unit thickness of a medium is expressed by the constant known as linear attenuation coefficient (LAC). It contains every conceivable interaction. LAC (μ) increases with increasing atomic number and physical density of absorbing material. LAC decreases with increasing photon energy except at K-edges (McKetty, 1998). The percentage of photons eliminated from a beam by an absorber per unit mass is expressed by the constant called mass attenuation coefficient (MAC). It is equal to the LAC divided by the absorber's density, i.e. $\mu_m = \frac{\mu}{\rho}$. MAC gives the probability of gamma ray interaction with the samples (Beutel *et al.*, 2000).

Half value layer (HVL) stands for the thickness of an absorbing material required to reduce the intensity of the radiation traveling through it by fifty percent. It is given by $HVL = \frac{0.693}{\mu}$ (Subedi *et al.*, 2023). As the absorber's atomic number rises, the half value layer falls. The tenth value layer (TVL) refers to the thickness of an absorber that reduces radiation intensity by a factor of a tenth of its initial value. It is expressed as $TVL = \frac{2.302}{\mu}$ (Sahadath *et al.*, 2015).

The average distance a moving particle travels before interacting with another particle and changing its direction or energy is known as the mean free path (mfp). The value of mfp depends upon the energy of photons and the nature of absorbing materials. The value of mfp is given as $1/\mu$ (Ahmed, 2015).

Due to the multiple partial photon interaction processes with matter, which require different weightings for the different atomic numbers in the material, effective atomic number is an energy-dependent characteristic. In some circumstances, such as creating radiation shielding, calculating absorbed dosage, energy absorption, and build-up factor, effective atomic number is also a useful statistic that conveniently depicts radiation interaction with matter (Kurudirek *et al.*, 2010).

The buildup factor refers to the different quantities of interest such as exposure to the interacting material. It is defined as the ratio of the quantity of interest due to total flux to the quantity of interest due to unscattered flux. The Beer-Lambert law has to meet the requirements of monochromatic ray, thin absorbing substance, and narrow beam geometry. If any of the aforementioned requirements are not followed, this law will be no longer active. By including the buildup factor (B), the law can be modified as $I = BI_0 e^{-\mu x}$ (Sayyed *et al.*, 2018). The significant changes in energy absorption buildup factor (EABF) and exposure buildup factor (EBF) are due to the variations in chemical compositions in the material and photon energy. EABF and EBF for gamma rays can be calculated by using five parameter geometric progression (GP) fitting formula (Subedi and Lamichhane, 2023).

The effective fast neutrons removal cross-section (FNRC) denoted by Σ_R is the probability that a fast neutron undergoes specific collisions per unit length of the interacting material. It is a parameter required to measure the neutron absorbing capacity of any material. It can be expressed in terms of partial density and mass-removal cross-section of the composite material (Sakar *et al.*, 2020).

The effect of ions like proton (H^1) and alpha particle (He^{+2}) on the interacting materials can be studied in terms of mass stopping power (MSP) and projected range (PR). MSP (MeVcm²/mg) is calculated by using the Bethe-Bloch formula and the general scheme of deducing PR (μ m) can be found in earlier literature (Kamisliloglu, 2021).

MATERIALS AND METHODS

The investigation of the effect of glass fiber content on the mechanical properties of cast polyamide has been carried out (Cuvalci *et al.*, 2014). By using an injection molding process, a number of cast polyamide-based composite materials were created. Cast polyamide and short glass fiber were utilized as the matrix and

reinforcement components in the creation of composite materials, respectively. Tests were performed on the specimens made from composite materials with various fiber contents to ascertain the density, elastic modulus, tensile elongation, and tensile and impact strengths of the composites. Additionally, research using scanning electron microscopy was done on the fracture surfaces of impact test specimens. However, the radiation

shielding features of these composites are yet to be studied. This work focuses on nuclear radiation shielding properties of E-glass fiber (SiO₂-Al₂O₃-B₂O₃-MgO-CaO-Na₂O-K₂O) reinforced cast polyamide (C₁₂H₂₂N₂O₂). The samples with chemical compositions and experimental densities have been presented in Table 1.

Table 1. Chemical compositions and densities of samples (Cuvalci *et al.*, 2014).

Sample	Chemical compositions (wt %)								Density (ρ) (g/cm ³)
	SiO ₂	Al ₂ O ₃	B ₂ O ₃	MgO	CaO	Na ₂ O	K ₂ O	C ₁₂ H ₂₂ N ₂ O ₂	
S1	5.24	1.44	1.06	0.46	1.72	0.04	0.04	90	1.15
S2	10.48	2.88	2.12	0.92	3.44	0.08	0.08	80	1.19
S3	15.72	4.32	3.18	1.38	5.16	0.12	0.12	70	1.24
S4	20.96	5.76	4.24	1.84	6.88	0.16	0.16	60	1.30
S5	26.20	7.20	5.30	2.30	8.60	0.20	0.20	50	1.37
S6	31.44	8.64	6.36	2.76	10.32	0.24	0.24	40	1.54
S7	36.68	10.08	7.42	3.22	12.04	0.28	0.28	30	1.73

The radiation shielding parameters were calculated using Phy-X/PSD online software. Photon Shielding and Dosimetry (PSD) software has been developed for the calculations of parameters pertinent to shielding and dosimetry. These variables include mean free path (mfp), effective atomic number and electron density (Z_{eff} , N_{eff}), effective conductivity (C_{eff}), half and tenth value layers (HVL, TVL), linear and mass attenuation coefficients (LAC, MAC), energy absorption, and exposure buildup factors (EABF, EBF). The fast neutron removal cross-section (FNRCs), another measure related to shielding, can also be estimated for a molecule or a mixture using Phy-X/PSD. Data on shielding parameters in the continuous energy range (1 keV–100 GeV) can be generated using this software (Sakar *et al.*, 2020). The energy range selected in this study was 0.015-15 MeV for the calculation of parameters. Further, the mass stopping power (MSP) and projected range (PR) parameters of glass fiber reinforced cast polyamide for alpha and proton particles were determined using SRIM-2008 codes.

RESULTS AND DISCUSSION

The shielding parameters were obtained within the energy range of 0.015-15 MeV with the application of Phy-X/PSD. The results obtained are graphically presented and discussed. The variation of the attenuation coefficients: LAC (μ) and MAC (μ_m) of the selected materials as a function of photon energy are presented in Fig. 1. Mainly, there are three photon-matter interaction phenomena, namely, photoelectric absorption, Compton scattering, and pair production. Based on the dominance of these phenomena, the changing trends of the attenuation coefficients can be explained. The maximum value of the attenuation coefficient in lower energy is due to photoelectric

absorption. Photoelectric absorption is a dominant process of X-ray absorption at lower photon energies (up to 0.5 MeV). In both intermediate and high energy regions, a steady decrement in the attenuation coefficients is observed. Among the samples selected, S7 is seen to possess higher values of attenuation coefficients. At 0.015 MeV, the values of MAC and LAC are, respectively, 5.880 cm²/g and 10.173 cm⁻¹. But, at the energy range 0.15-4 MeV, slightly higher values of MAC are observed for S1. The zoomed portion in Fig. 1 depicts a slight dominance in higher MAC values by S1 at the intermediate region. Sample S1 possesses the lower values of MAC and LAC at 0.015 MeV, the values being 1.666 cm²/g and 1.916 cm⁻¹. The values of LAC for S1 at all photon energies are found to be lower among all the taken samples. This shows that LAC is a density-dependent parameter whereas MAC is not.

HVL and TVL are widely used concepts in shielding design. The HVL and TVL help in calculating the thickness of the layer for achieving acceptable reduction. Since LAC itself is density-dependent, it can be understood that the parameters HVL and TVL depend upon the density of the material used. Similarly, mfp is also a density-dependent parameter as it can be understood as the reciprocal of LAC. The variations of HVL, TVL, and mfp as a function of photon energy are depicted in Fig. 2. We can observe a similar trend in the variation of HVL, TVL, and mfp with photon energy for all the samples. S7 requires a lower layer thickness for attenuation of photons than other samples whereas S1 requires larger layer thickness. Also, S7 exhibits lower values of mfp among the samples and S1 exhibits higher values. The general order of HVL, TVL, and mfp values for the samples can be presented as S7 < S6 < S5 < S4 < S3 < S2 < S1.

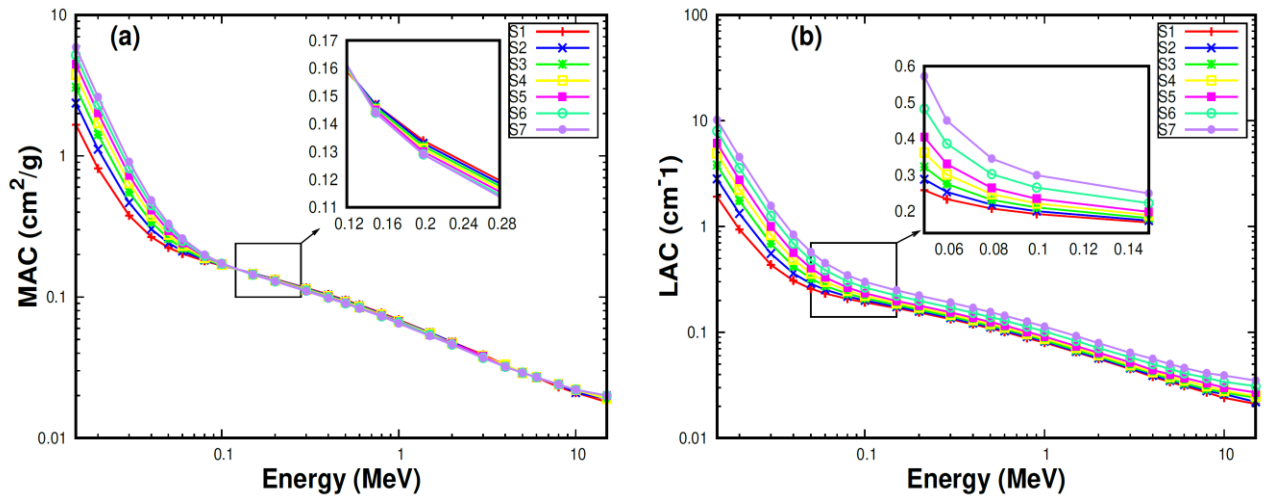


Figure 1. Changing features of (a) MAC (μ_m), and (b) LAC (μ) as the function of photon energy.

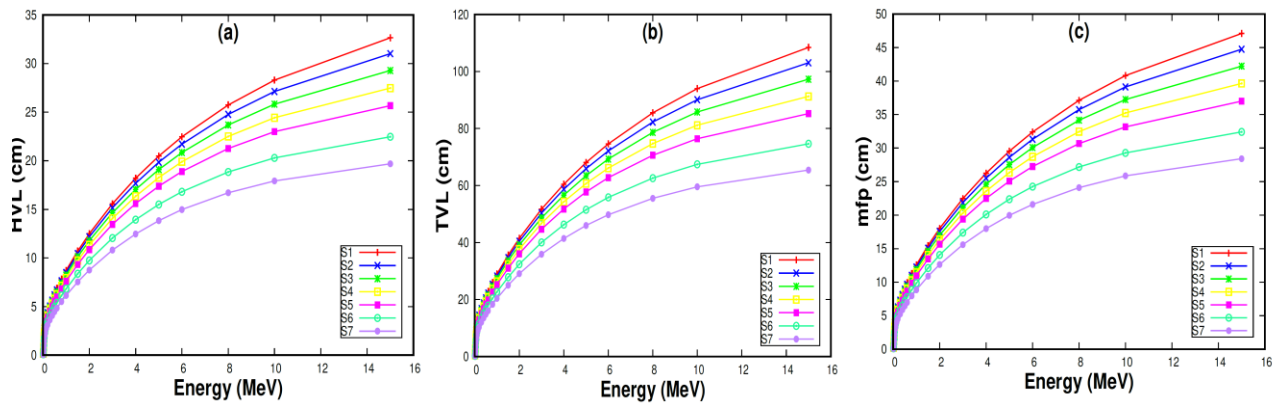


Figure 2. Variations of (a) HVL, (b) TVL, and (c) mfp as the function of energy.

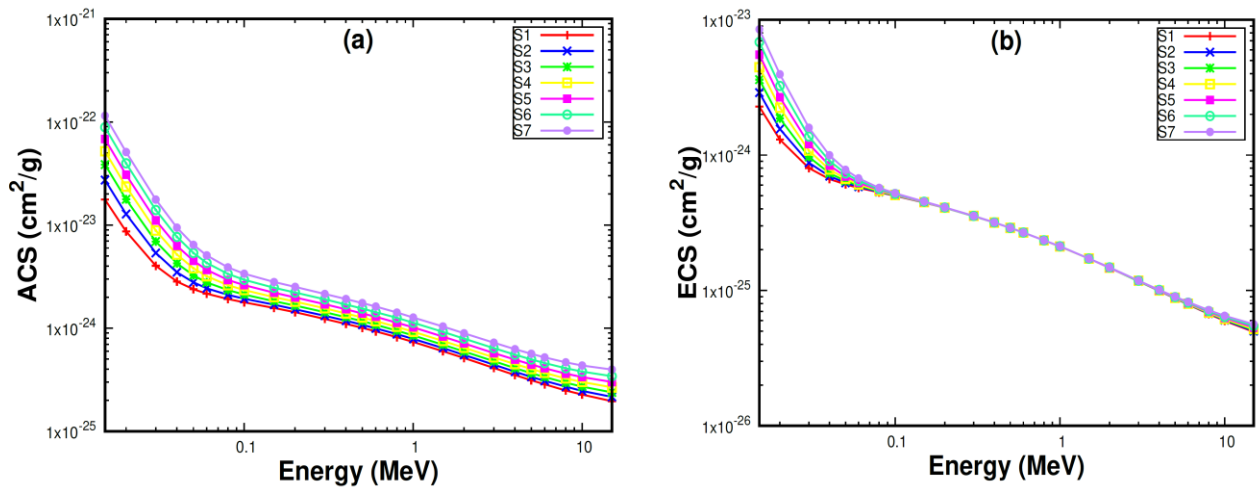


Figure 3. Variations of (a) ACS and (b) ECS with energy of radiation.

Particularly at 1 MeV photon energy, for S1 to S7, the values of HVL are respectively 8.719, 8.505, 8.239, 7.934, 7.601, 6.828, and 6.138 cm. At the same energy, the values of TVL are respectively 28.962, 28.252,

27.369, 26.356, 25.251, 22.683 and 20.390 cm and the mfp values are 12.578, 12.270, 11.886, 11.446, 10.966, 9.851, and 8.855 cm. Based on the values of HVL, TVL, and mfp, S7 can be considered the better shield agent

among the given samples. Atomic cross-section (ACS) and electronic-cross section (ECS) are the parameters that provide the probability of radiation interactions per atom and per electron, respectively, in each unit volume of shielding material. A larger cross-section implies a larger probability of collision between incident photons and the atoms. The variation of ACS and ECS as a function of energy of radiation is presented in Fig. 3.

At all energies, the ACS values for the samples are observed in pattern $S1 < S2 < S3 < S4 < S5 < S6 < S7$. However, between 0.3-3 MeV, almost equal ECS values are observed for the samples. After 2 MeV, the ECS values vary similarly to that of ACS. This shows that

ECS not only depends on the energy of radiation but also the composition of the samples taken. Based on the ACS and ECS values, S7 can be considered as the better radiation shielding material, and S1 is the least suitable among the samples.

Higher effective atomic number EAN (Z_{eff}) materials are preferred when they are used for radiation shielding. A higher value of Z_{eff} ensures a higher probability of photon collisions with the substances. Fig. 4(a) depicts the change in Z_{eff} as a function of the energy of radiation.

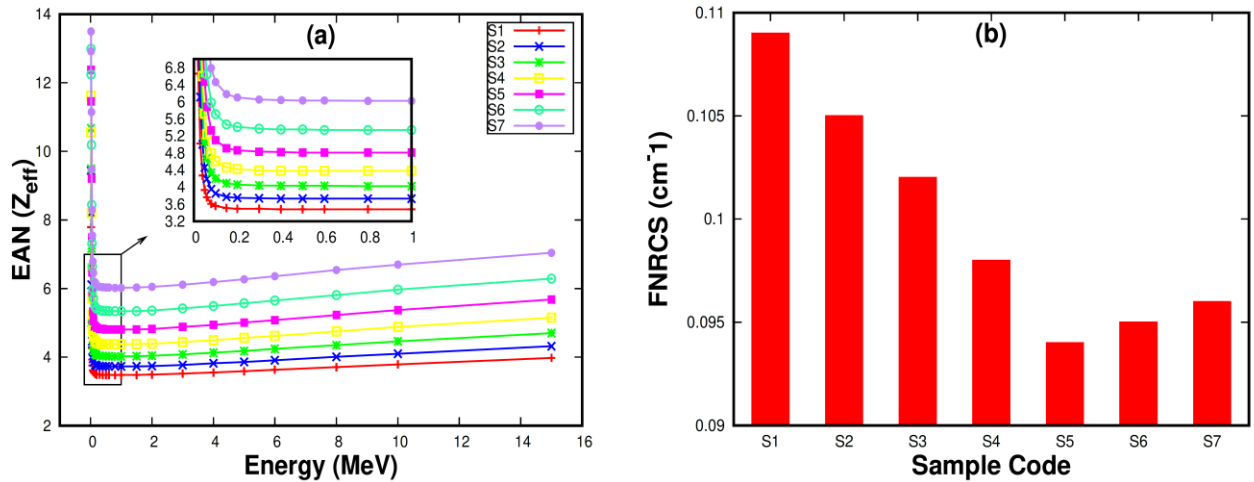


Figure 4. (a) Plots for EAN (Z_{eff}) as the function of radiation energy, (b) FNRCs of all selected samples.

Higher values of Z_{eff} are observed at 0.015 MeV for all samples. The maximum Z_{eff} values observed for samples S1-S7 respectively are 7.79, 9.44, 10.67, 11.62, 12.38, 12.99, and 13.50. There is an abrupt decreasing nature of Z_{eff} up to 0.15 MeV radiation energy. After which stable values are observed till 1.5 MeV. Further increment of radiation energy resulted in the increasing values of Z_{eff} . This can be explained based on the various photon-matter interactions dominant regions. The photoelectric effect interaction index depends on the fifth power of Z_{eff} whereas the Compton scattering, and pair production interaction indices are, respectively, related to Z_{eff} and its square. Thus, there is a sharp decline in Z_{eff} at photoelectric absorption dominant region, a stable nature in the Compton scattering dominant region and a slight increase in the pair production region. Particularly at 1 MeV, the observed values of Z_{eff} for samples S1-S7 respectively are 3.48, 3.73, 4.02, 4.38, 4.81, 5.34, and 6.02. These are the minimum values of Z_{eff} observed for the samples. S7 among all the samples exhibits higher values of Z_{eff} whereas S1 holds smaller values. FNRCs (Σ_R) is of great significance when the material is used in shielding the nuclear reactors where nuclear fission takes place in the

presence of neutrons. The values of Σ_R are presented in Fig. 4(b). The Σ_R values for the samples S1-S7 are 0.109, 0.105, 0.102, 0.098, 0.094, 0.095, and 0.096 cm^{-1} respectively. S1 has the highest value of FNRCs among the samples whereas S5 has the lowest value. It indicates that the higher molecular weight plays an important role in high-energy neutron shielding. Hence, S1 would be the most effective shield for fast neutrons and S5 would be the least effective.

The exposure buildup factor (EBF) for the samples up to 35 mfp has been calculated using the G-P fitting method in the selected energy range 0.015-15 MeV. The change in EBF with incident photon energy at penetration depths of 5, 10, 15, 20, 25, 30, and 35 mfp for samples S1-S7 are presented in Fig. 5 (a-g). The EBF values for all samples rise to a maximum value at intermediate energies before beginning to fall. The predominant photon interaction activity in the low energy area is the photoelectric effect, whose cross-section varies inversely with energy as $E^{-3.5}$. The largest number of photons will be absorbed by the materials as a result of the dominance of the photoelectric effect. As a result, the EBF value in the lower energy zone decreases. Compton scattering, which is a major photon

interaction activity in the region of intermediate energy, only contributes to the loss of photon energy owing to scattering and is unable to totally remove the photon. Because the photon's lifetime is longer in this energy range, there is a greater chance that it will escape from the shielding material. EBF value rises as a result of this procedure. Another photon absorption process, pair production, which has a cross-section that varies inversely with energy as E^2 , is prominent in the higher energy area. Thus, in higher energy regions, the value of EBF decreases again. Higher EBF values are observed at higher penetration depth for the selected samples. The variation in buildup factor with chemical compositions has also been studied. Fig. 5(h) depicts the variation of EBF with radiation energy of all selected samples at 35 mfp penetration depth. It is seen that the sample with the lowest Z_{eq} (S1) dominates the maximum values of EBF whereas the sample with the highest Z_{eq} (S7) dominates the minimum values of EBF. At 35 mfp penetration depth, the lowest EBF for S7 is found to be

1.18 at 0.015 MeV incident energy. However, at 3 MeV, S3, S4 and S5 exhibits smaller EBF values. Above 3 MeV, S1 exhibits the lower EBF values among the samples. Thus, S7 would be a better shield at lower energy regions and S1 would be a better shield at higher energy regions.

Fig. 6 demonstrates the variation of EBF with penetration depth at fixed energy. An increasing trend of EBF is observed with increasing penetration depth. The scattered photon multiplication coefficient as well as the likelihood of Compton scattering increases with the increase in penetration depth. This causes the rise in EBF. At 1 MeV, S7 possesses lower EBF values thus proving to be a better radiation shielding material. But, at 3 MeV, up to 20 mfp penetration depth, S7 exhibits lower EBF values. At 25 mfp depth, S5 shows lower EBF value and S4 shows lower EBF values at 30 and 35 mfp penetration depths.

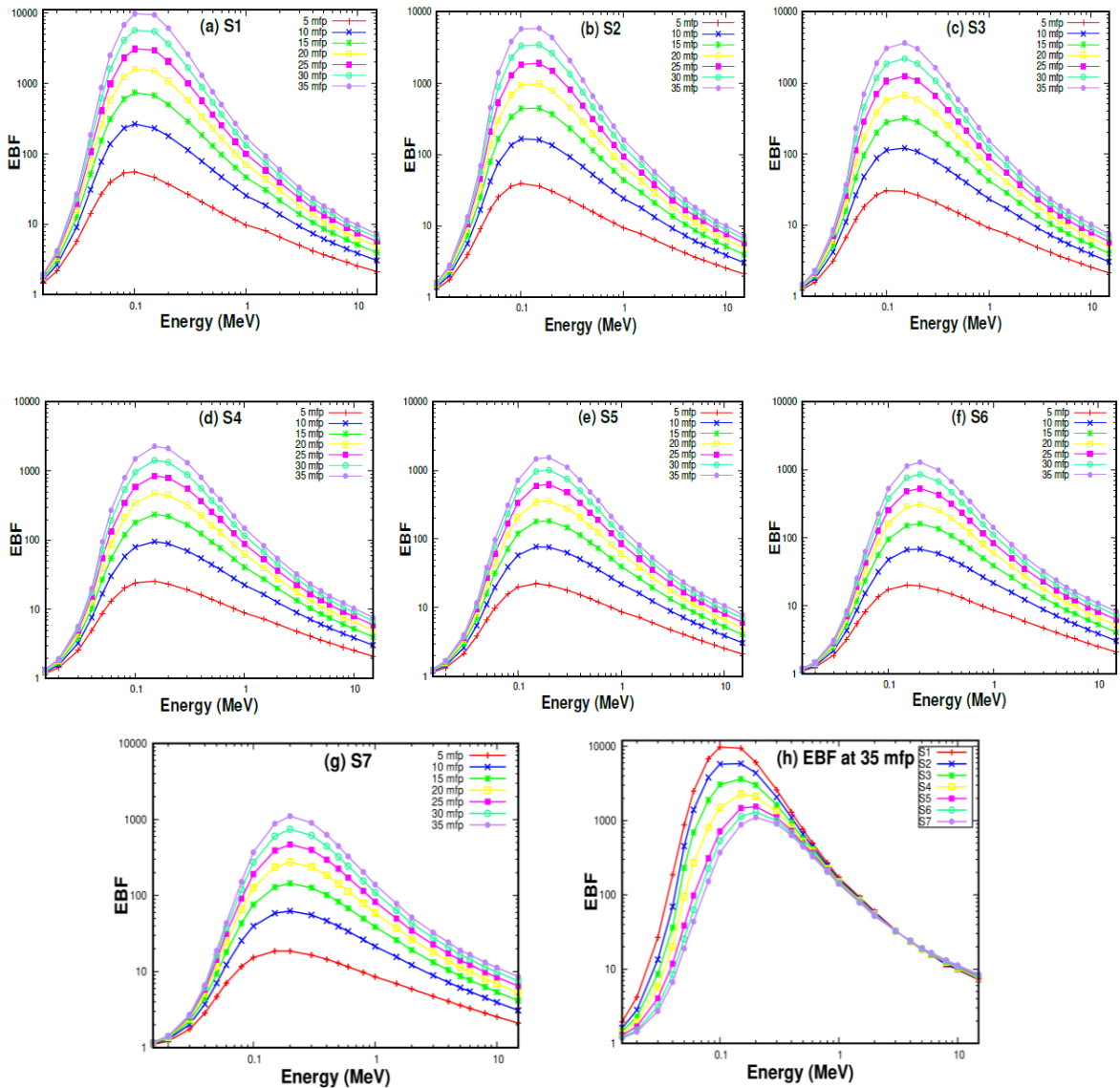


Figure 5. Plots for EBF as the function of photon energy for samples S1-S7 (a-g) at various penetration depths, and (h) at 35 mfp penetration depth.

Finally, the mass stopping power (MSP) and projected range (PR) parameters of glass fiber reinforced cast polyamide for alpha and proton particles were determined using SRIM-2008 codes. A charged particle's linear stopping power is defined as the rate of energy loss per unit length of motion. By dividing the linear stopping power by the material density, one can determine the mass stopping power (MSP). The projected range (PR) is the maximum distance a charged particle can travel before losing kinetic energy (Perişanoğlu *et al.*, 2019). Fig. 7 (a-b) illustrates the change in MSP as a function of kinetic energy for proton and alpha particles. The minimum values of MSP are obtained for S7. The MSP values gradually increase up

to 0.07 MeV of kinetic energy after which the values drastically fall for proton whereas the values reach the maximum for alpha particle at about 0.6 MeV. The range (PR) of charged particles within the material is another major parameter. Fig. 8 (a-b) provides the variation of PR values for proton and alpha particles with kinetic energy. The PR values of all samples for alpha particle and proton exhibit an increasing trend with the kinetic energy. The smallest values of PR are preferred. S7 and S6 show the smallest PR values for both proton and alpha particles due to their high densities whereas S1 and S2 exhibited higher values. Eventually, S7 could be preferred as a shielding material for the protection of gamma, neutron, proton, and alpha radiation.

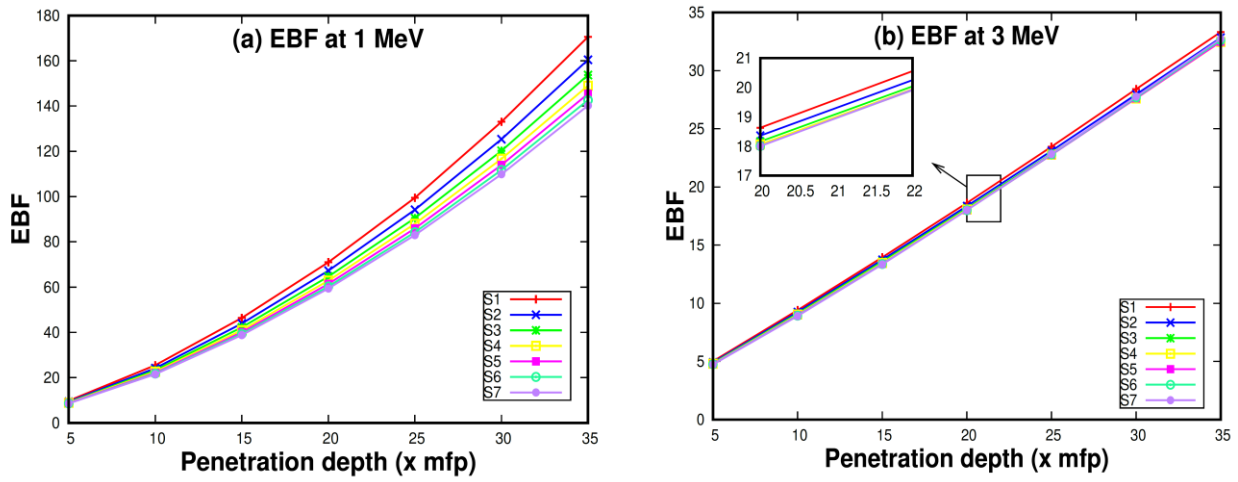


Figure 6. Plots for EBF as the function of penetration depth at (a) 1 MeV, and (b) 3 MeV.

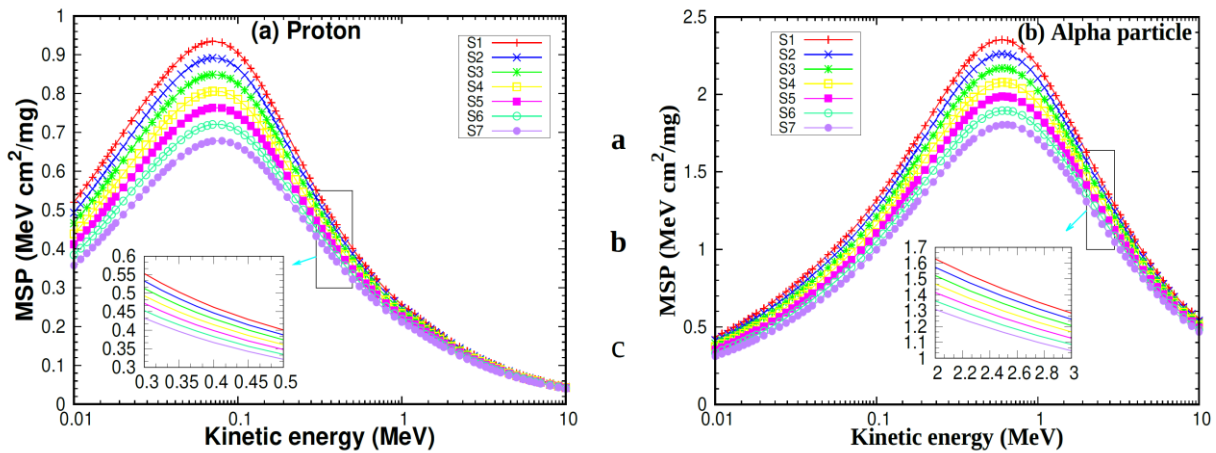


Figure 7. Variation of (a) proton and (b) alpha mass stopping power (MSP) as a function of kinetic energy.

The mechanical characteristics of cast-polyamide-based composites can be enhanced by adding reinforcement materials and fillers to the polymer matrix. The results obtained suggest that the addition of E-glass fiber contents in the cast-polyamide increases the effectiveness of the material in radiation shielding applications. Similar results were found in inspecting the electromagnetic shielding effectiveness (EMSE) of copper glass fiber knitted fabric reinforced polypropylene composites (Cheng *et al.*, 2000). The amount of copper in the composite material had a

significant impact on the EMSE of knitted composites. The conductive knitted composite's electromagnetic shielding abilities were found promising. Similarly, the radiation attenuation parameters varied significantly, strongly influenced by the amount of bismuth nitrate pentahydrate (BNP) used as filler in the polycarbonate matrix (Mirji and Lobo, 2020). The X-ray shielding properties of gadolinium oxide/poly-ether-ether-ketone composites improved with the increment of gadolinium oxide (Wang *et al.*, 2015).

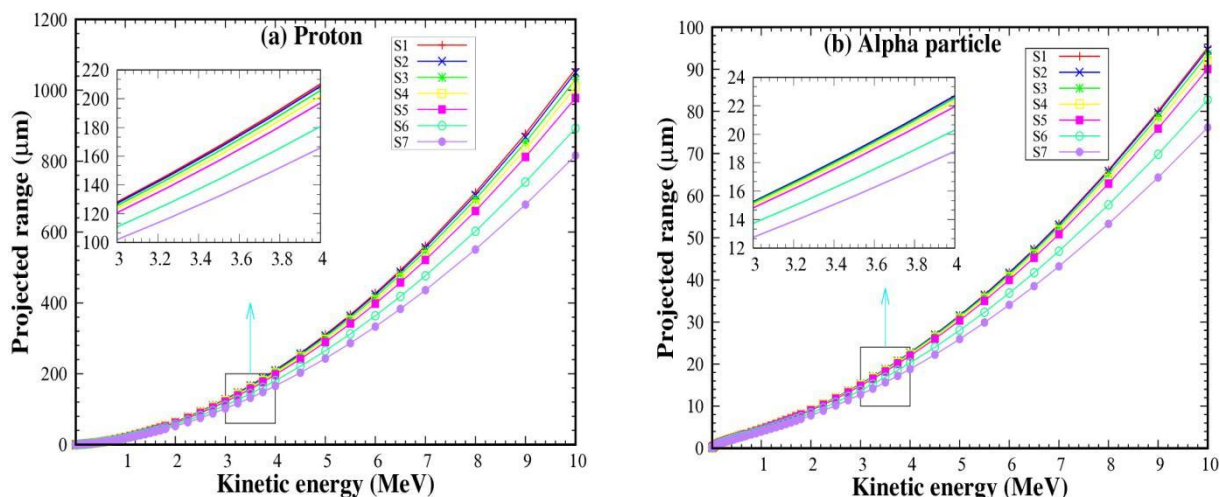


Figure 8. Variation of (a) proton and (b) alpha projected range (PR) as a function of kinetic energy.

Table 2 illustrates the results for HVL and mfp in comparison to other materials in the literature at 100 keV. Lower values of HVL and mfp for S7 indicate better attenuation abilities than molybdenum carbide (15% by weight) reinforced high-density polyethylene (HDPE) and tungsten (1% by weight) reinforced light density polyethylene (LDPE). However, concrete shows lower values of HVL and mfp indicating its greater effectiveness in radiation shielding applications than glass fiber-reinforced cast polyamide.

There has been widespread use of E-glass fiber as a reinforcing agent in various composites due to its unique features like excellent flexibility, high tensile strength, low thermal conductivity, and excellent electrical insulation properties. The fields of application of glass fiber reinforced polyamides include construction, transportation, infrastructure, and consumer goods. This research recommends the use of glass fiber reinforced cast polyamide in low-energy radiation shielding.

Table 2. Comparison of results obtained with other materials at 100 keV.

Study	Study theme	Composites	HVL (cm)	mfp (cm)
This study	Simulation	S7 (glass fiber 70%+cast polyamide 30%)	2.31	3.34
(Almurayshid <i>et al.</i> , 2021)	Experiment	HDPE+MoC 15%	2.52	3.63
(Alavian & Tavakoli-Anbaran, 2019)	Simulation	LDPE+W 1%	-	4.27
(Gurler & Akar-Tarim, 2016)	Simulation	Concrete (NBS)	1.81	2.62

CONCLUSIONS

The radiation shielding features for glass fiber reinforced cast polyamide were investigated using Phy-X/PSD in the energy range 0.015-15 MeV. The neutron shielding capabilities as well as the exposure buildup factor of the materials were also determined. S7 (70% glass fiber content) is observed to have the higher values of LAC, MAC, and Z_{eff} whereas the lower values of HVL, TVL and mfp. S1 (10% glass fiber content) possessed lower values of MAC, LAC, Z_{eff} and higher values of HVL, TVL, mfp, and FNRCs. In the intermediate energy regions, the minimum EBF values are dominated by S7. However, at higher energy region, S1 dominated the minimum EBF values. Based on the results, it can be concluded that S7 would provide much more efficiency in radiation shielding among the samples whereas for fast neutron shielding, S1 would be the best material. The increase in concentration of glass fiber resulted in

better radiation shielding features of glass fiber reinforced cast polyamide. According to the MSP and PR measurements carried out using SRIM-2008 codes, the proton and alpha energies both reduced more as they passed through sample S7. The outcomes obtained imply that the cast-polyamide's radiation shielding capabilities are improved by the inclusion of E-glass fiber contents. The use of E-glass fiber reinforced cast polyamide is encouraged in low-energy radiation shielding in medical and industrial fields. Radiation protection garments could be constructed using E-glass fiber reinforced cast polyamide instead of dense materials which ensures more comfort and flexibility. However, it is essential to consider the energy of radiation and the thickness of the shielding material.

AUTHOR CONTRIBUTIONS

JP worked out the theoretical backgrounds and did the measurements of radiation shielding parameters

employing Phy-X/PSD. BS carried out the calculations of MSP and PR using SRIM software. TRL suggested tools, checked results and plots, revised the draft manuscript, and finalized the manuscript before submission.

CONFLICT OF INTEREST

The authors declare no conflict of interest.

DATA AVAILABILITY STATUS

Upon reasonable request, the data that supports this study will be made available by the authors.

REFERENCES

- Ahmed, S.N. (2015). *Physics and engineering of radiation detection*. Second Edition, Elsevier, New York.
- Alavian, H., Samie, A., & Tavakoli-Anbaran, H. (2020). Experimental and Monte Carlo investigations of gamma ray transmission and buildup factors for inorganic nanoparticle/epoxy composites. *Radiation Physics and Chemistry*, *174*, 108960.
- Alavian, H., & Tavakoli-Anbaran, H. (2019). Study on gamma shielding polymer composites reinforced with different sizes and proportions of tungsten particles using MCNP code. *Progress in Nuclear Energy* *115*, 91–98.
- Al-Buriahi, M.S., Sriwunkum, C., Arslan, H., Tonguc, B.T., & Bourham, M.A. (2020). Investigation of barium borate glasses for radiation shielding applications. *Applied Physics A*, *126*, 68.
- Almurayshid, M., Alsagabi, S., Alssalim, Y., Alotaibi, Z., & Almsalam, R. (2021). Feasibility of polymer-based composite materials as radiation shield. *Radiation Physics and Chemistry*, *183*, 109425.
- Ambika, M.R., Nagaiah, N., & Suman, S.K. (2017). Role of bismuth oxide as a reinforcer on gamma shielding ability of unsaturated polyester based polymer composites. *Journal of Applied Polymer Science*, *134*(13), 44657.
- Beutel, J., Kundel, H.L., & Van Metter, R.L. (2000). *Handbook of medical imaging*. SPIE Press, Bellingham.
- Cheng, K.B., Ramakrishna, S., & Lee, K.C. (2000). Electromagnetic shielding effectiveness of copper/glass fiber knitted fabric reinforced polypropylene composites. *Composites Part A: Applied Science and Manufacturing*, *31*(10), 1039-1045.
- Cuvalci, H., Erbay, K., & Ipek, H. (2014). Investigation of the effect of glass fibre content on the mechanical properties of cast polyamide. *Arabian Journal for Science and Engineering*, *39*, 9049-9056.
- El-Denglawey, A., Alshammari, H., Tekin, S., AbuShanab, W., & Saddeek, Y. (2021). Prediction of mechanical and radiation parameters of glasses with high Bi₂O₃ concentration, *Results in Physics*, *21*, 103839.
- El-Mallawany, R. (2018). Radiation shielding properties of tellurite glasses. In El-Mallawany, R. (Ed.), *Tellurite Glass Smart Materials: Applications in Optics and Beyond* (pp. 17-27), Springer.
- Galante, A.M.S., & Campos, L.L. (2010). Characterization of polycarbonate dosimeter for gamma-radiation dosimetry.
- Gurler, O., & Akar-Tarim, U. (2016). Determination of radiation shielding properties of some polymer and plastic materials against gamma-rays. *Acta Physica Polonica A* *130* (1), 236–238.
- Hussein, K.I., Alqahtani, M.S., Meshawi, A.A., Alzahrani, K.J., Zahran, H.Y., Alshehri, A.M., Yahia, I.S., Reben, M., & Yousef, E.S. (2022). Evaluation of the radiation shielding properties of a tellurite glass system modified with sodium oxide. *Materials*, *15*(9), 3172.
- Kamislioglu, M. (2021). An investigation into gamma radiation shielding parameters of the (Al: Si) and (Al+ Na): Si-doped international simple glasses (ISG) used in nuclear waste management, deploying Phy-X/PSD and SRIM software. *Journal of Materials Science: Materials in Electronics*, *32*(9), 12690-12704.
- Kurudirek, M., Büyükyıldız, M., & Özdemir, Y. (2010). Effective atomic number study of various alloys for total photon interaction in the energy region of 1keV–100GeV. *Nuclear Instruments and Methods in Physics Research Section A: Accelerators, Spectrometers, Detectors and Associated Equipment*, *613*, 251-256.
- McKetty, M.H. (1998). The AAPM/RSA physics tutorial for residents. X-ray attenuation. *Radiographics*, *18*, 151-163.
- Mirji, R., & Lobo, B. (2020). Study of polycarbonate–bismuth nitrate composite for shielding against gamma radiation. *Journal of Radioanalytical and Nuclear Chemistry*, *324*(1), 7-19.
- More, C.V., Alsayed, Z., Badawi, M.S., Thabet, A.A., & Pawar, P.P. (2021). Polymeric composite materials for radiation shielding: a review. *Environmental Chemistry Letters*, *19*, 2057–2090.
- Nagaraja, N., Manjunatha, H., Seenappa, L., Sridhar, K., & Ramalingam, H. (2020). Radiation shielding properties of silicon polymers. *Radiation Physics and Chemistry*, *171*, 108723
- Perişanoğlu, U., El-Agawany, F., Kavaz, E., Al-Buriahi, M., & Rammah, Y. (2019). Surveying of Na₂O₃–BaO–PbO–Nb₂O₅–SiO₂–Al₂O₃ glass-ceramics system in terms of alpha, proton, neutron and gamma protection features by utilizing GEANT4 simulation codes. *Ceramics International*, *46*(3), 3190-3202.
- Sahadath, H., Mollah, A.S., & Huq, F. (2015). Calculation of the different shielding properties of locally developed ilmenite-magnetite (I-M) concrete. *Radioprotection*, *50*(3), 203-207.
- Sakar, E., Ozpolat, O.F., Alim, B., Sayyed, M.I., & Kurudirek, M. (2020). Phy-X / PSD: Development of a user friendly online software for calculation of parameters relevant to radiation shielding and dosimetry. *Radiation Physics and Chemistry*, *166*, 108496.
- Sayyed, M.I., AlZaatreh, M.Y., Matori, K.A., Sidek, H.A.A., & Zaid, M.H.M. (2018). Comprehensive study on estimation of gamma-ray exposure buildup factors for smart polymers as a potent application in nuclear industries. *Results in Physics*, *9*, 585-592.

- Subedi, B., Paudel, J., & Lamichhane, T.R. (2023). Gamma-ray, fast neutron and ion shielding characteristics of low-density and high-entropy Mg-Al-Ti-V-Cr-Fe-Zr-Nb alloy systems using Phy-X/PSD and SRIM programs. *Heliyon*, 9(7), e17725.
- Subedi, B., & Lamichhane, T.R. (2023). Radiation shielding properties of low-density Ti-based bulk metallic glass composites: a computational study. *Physica Scripta*, 98(3), 035003.
- Wang, H., Zhang, H., Su, Y., Liu, T., Yu, H., Yang, Y., Li, X., & Guo, B. (2015). Preparation and radiation shielding properties of Gd₂O₃/PEEK composites. *Polymer Composites*, 36(4), 651–659.
- Ziegler, J.F., Ziegler, M.D., & Biersack, J.P. (2010). SRIM – The stopping and range of ions in matter. *Nuclear Instruments and Methods in Physics Research Section B: Beam Interactions with Materials and Atoms* 268, 1818-1823.